2016

Neodymium-Based Stoichiometric Ultrasmall Nanoparticles for Multifunctional Deep-Tissue Photothermal Therapy

Blanca del Rosal, Alberto Perez-Delgado, Elisa Carrasco, Dragana J. Jovanović, Miroslav Dramićanin, Goran Dražić, Angeles Juarranz de la Fuente, Francisco Sanz-Rodriguez, Daniel Jaque

Published in:

Advanced Optical Materials

DOI:
10.1002/adom.201500726

Document version:
Peer reviewed article (often known as postprint article)

Recommended citation:
del Rosal, B., Pérez-Delgado, A., Carrasco, E., Jovanović, D. J., Dramićanin, M. D., Dražić, G., ... & Jaque, D. (2016). Neodymium-Based Stoichiometric Ultrasmall Nanoparticles for Multifunctional Deep-Tissue Photothermal Therapy. Advanced Optical Materials, 4(5), 782-789.

DOI: 10.1002/ ((please add manuscript number))
Article type: Full Paper

Title Neodymium-based stoichiometric ultrasmall nanoparticles for multifunctional deep-tissue photothermal therapy

*Blanca del Rosal, Alberto Pérez-Delgado, Elisa Carrasco, Dragana Jovanović, Miroslav D. Dramićanin, Goran Dražić, Ángeles Juarranz de la Fuente, Francisco Sanz-Rodríguez, and Daniel Jaque **

B. del Rosal, A. Pérez-Delgado, Dr. D. Jaque
Fluorescence Imaging Group, Departamento de Física de Materiales, Facultad de Ciencias, Universidad Autónoma de Madrid, Madrid 28049, Spain.
E-mail: d. jaque@uam.es

Dr. E. Carrasco
Instituto de Investigaciones Biomédicas "Alberto Sols", CSIC-UAM, Madrid 28029, Spain
Grupo de Dermatología Experimental, Instituto Ramón y Cajal, Madrid 28034, Spain

Dr. D. Jovanović, Prof. M. D. Dramićanin
University of Belgrade, Vinča Institute of Nuclear Sciences, P.O. Box 522, 11001, Serbia

Dr. G. Dražić
Laboratory for Materials Chemistry, National Institute of Chemistry, Hajdrihova 19, 1000 Ljubljana, Slovenia

Prof. A. Juarranz de la Fuente, Dr. F. Sanz-Rodríguez
Departamento de Biología. Facultad de Ciencias, Universidad Autónoma de Madrid, Madrid 28049, Spain

Dr. Francisco Sanz-Rodríguez, Dr. D. Jaque
Instituto Ramón y Cajal de Investigación Sanitaria IRYCIS, Ctra. Colmenar km. 9.100, Madrid 28034 , Spain

Keywords: Rare earth nanoparticles, photothermal therapy, fluorescence imaging, ultrasmall nanoparticles

Nanoparticle-mediated photothermal therapy (NP-PTT) constitutes a flexible, highly selective, cost effective and accurate tool for cancer treatment alone or in combination with other therapies such as radiotherapy or chemotherapy. The future application of NP-PTT in real life mainly depends on the design and synthesis of novel multifunctional nanoparticles that could overcome the current limitations of NP-PTT such as limited penetration depth and absence of therapy control. In this work we report on ultrasmall (~2.4 nm) $NdVO_4$ stoichiometric (100 %

constituent Nd^{3+} ions) nanoparticles capable, under 808 nm optical excitation, of in vivo sub-tissue localized heating while providing, simultaneously, the possibility of high penetration near-infrared fluorescence imaging. Ultrasmall $NdVO_4$ stoichiometric nanoparticles have evidenced a superior light-to-heat conversion efficiency. This is explained in terms of their large absorption cross section at 808 nm (consequence of the particular spectroscopic properties of neodymium ions in $NdVO_4$ and of the high neodymium content) as well as to their ultrasmall size that leads to large non-radiative decay rates. Results included in this work introduce to the scientific community ultrasmall $NdVO_4$ stoichiometric nanoparticles as multifunctional photothermal agents that could be considered as an alternative to traditional systems such as metallic, organic or carbon-based nanoparticles.

1. Introduction

Thermal therapy, which relies on heat as a means to cause cell death, has been widely explored in the past as a minimally invasive tool to treat different diseases, including malignant tumors.[1] In order to maximize the efficacy of the therapy and to simultaneously minimize the undesirable collateral damage, the tumor must be heated up to cytotoxic levels while keeping the heating at the surroundings at a minimum.[2] Such selectivity has been achieved by using photothermal nanoparticles (PT-NPs), capable of efficient heat generation under optical excitation. Nanoparticle-assisted photothermal therapy (NP-PTT) consists on the selective incorporation of heating NPs inside the tumor to be treated in such a way that a subsequent optical excitation would produce a well localized heating of the tumor. NP-PTTs have already been used for in vivo cancer treatment in animal models with remarkable success.[3] Although a great variety of nanostructures, ranging from gold NPs to carbon-based nanomaterials and even organic NPs, have been used as photothermal agents, the research on novel heating NPs capable of overcoming the actual limitations of NP-PTT is a hot area involving a large scientific community.[4] One of the most important limitations of

photothermal therapy is the light absorption and scattering of biological tissues, which results in a reduced penetration depth of the optical excitation radiation required for sub-tissue heat generation.[5] This limitation can be partially overcome by working with heating NPs with high absorption cross sections at wavelengths lying in the so-called biological windows (BWs). These BWs correspond to spectral ranges (700-900 nm, first BW, 1000-1400 nm, second BW and 1500-1800 nm, third BW) where tissues are partially transparent due to the simultaneous reduction of both absorption and scattering coefficients.[6] Besides allowing for a better penetration depth, working in the BWs also minimizes the light-induced damage in healthy tissues, as the optical excitation radiation will not be significantly absorbed by tissues, so that the energy deposition will be kept at a minimum.[7]

Rare earth-doped nanoparticles (RENPs), initially used as simple optical markers,[8] have been explored in the past few years as PT-NPs concluding that they could constitute a reliable alternative to the widely used metallic and carbon nanostructures.[9] In most of the cases, light-induced heating in RENPs is accompanied by the simultaneous generation of a fluorescence signal especially suitable for in vivo imaging.[10] This would be particularly interesting when analyzing the outcome of a photothermal therapy, as fluorescence imaging could be used to monitor the post-treatment evolution of the tumor. Furthermore, RENP fluorescence would also provide the possibility of tracking them in real time after thermal treatment, thus allowing to determine their biodistribution and clearance from the body.[11] In this context, neodymium (Nd^{3+}) arises as a most interesting doping ion for this type of NPs. First of all, Nd^{3+} ions can be efficiently excited by 808 nm radiation, which lies in the first biological window and is produced by cost-effective laser diodes. This excitation wavelength has also been demonstrated to be a “safe” wavelength in biological applications.[12] Moreover, Nd^{3+} ions characteristic emission bands (at around 890, 1060 and 1350 nm) all lie in the biological windows, which allow for deep-tissue imaging using an infrared camera.[13] Previous works have demonstrated high light-to-heat conversion efficiencies in heavily-doped

Nd^{3+}-doped RENPs (Nd:NPs) as a consequence of an enhancement in the absorption cross section together with a reduction in the fluorescence quantum yield (QY), respectively.[14] Up to now, different neodymium-doped fluoride nanocrystals with varying Nd^{3+} content have been studied for NP-PTT.[15] In particular, heavily-doped (5.6 at.%) Nd:LaF_3 NPs have been successfully used for self-monitored temperature controlled photothermal therapy.[16]

Previous studies have concluded that, while Nd:NPs display the already mentioned interesting properties (such as superior spectral and physical stabilities), they also present the disadvantage of a relatively low absorption cross section per NP, which results in a non-efficient absorption of optical excitation radiation.[3] Such reduced absorption cross section stems from the intrinsic low absorption probabilities characteristic of Nd^{3+} ions as well as from the typically low content of Nd^{3+} ions per RENP (usually below 10 mol.%). This limitation can be partially overcome by increasing the doping level, i.e., the content of rare earth ions per NP, as it would lead to an overall increase in the RENPs absorption cross section. Nevertheless, massive incorporation of Nd^{3+} ions in NPs is not an easy task as it typically causes a remarkable deterioration in the structural properties of Nd:NPs. Still, it is possible to find in the literature numerous examples of crystalline materials in which a complete substitution of constituent ions by Nd^{3+} ions is possible, leading to the so-called stoichiometric crystals (with a 100% mol. concentration of Nd^{3+} ions). Among all the Nd^{3+} doped stoichiometric systems reported up to now, neodymium orthovanadate ($NdVO_4$) seems to be particularly interesting. Neodymium-doped orthovanadate crystals show excellent mechanical and physical properties that are accompanied by an outstanding optical absorption at 808 nm, an especially desirable wavelength for biomedical applications, as explained above.[17] Despite their good bulk properties the potential application of $NdVO_4$ stoichiometric nanoparticles as PTT-NPs is still unexplored.

In this work, we have synthesized ultrasmall $NdVO_4$ stoichiometric NPs. Their infrared spectroscopic properties as well as their light-to-heat conversion capability have been

thoroughly investigated and results have been compared to those obtained for other Nd^{3+} doped PT-NPs. Ex vivo and in vivo experiments were conducted in order to corroborate their potential application of ultrasmall $NdVO_4$ stoichiometric NPs as multifunctional photothermal agents and imaging probes.

2. Results and discussion

2.1. Synthesis and characterization of $NdVO_4$ ultrasmall NPs

The ultrasmall $NdVO_4$ stoichiometric NPs used in this work were synthesized for the first time using the colloidal (citrate) synthetic route described in detail in the Experimental section. Although the fabrication of $NdVO_4$ NPs has already been reported, other synthesis procedures, such as sonochemical or (solvo-)hydrothermal were used, resulting in NPs with average sizes much larger than the ones presented in this work.[18] Inset in **Figure 1(a)** shows a characteristic high resolution STEM image of a representative group of $NdVO_4$ stoichiometric NPs. The statistical analysis of different STEM images, some of which are included in the Supporting Information (section S1) allowed us to build up the size histogram displayed in **Figure 1(a)** from which an average NP size of ~2.4 nm was determined. The crystalline character of the NPs was confirmed by X-Ray Diffraction (XRD), as is shown in section S2 of the Supporting Information.

Ultrasmall NPs, with sizes below 10 nm, have been reported to have significant advantages with respect to larger NPs for biological applications. In particular, they show better penetration into cells and are even able to penetrate the nuclear membrane, as demonstrated by in vitro experiments. Indeed, upon intravenous injection in mice with tumors, smaller NPs show longer blood circulation half-lives and much higher uptake by the tumors.[19] In our case, the ultrasmall size of NPs is accompanied by an outstanding colloidal character and remarkable stability, as no sign of precipitation or degradation was observed in the samples after months of storage. Aqueous dispersions of $NdVO_4$ stoichiometric NPs with

concentrations as high as 10% in mass were prepared without any sign of precipitation for months. **Figure 1(b)** includes, as an example, an optical image of an aqueous dispersion of $NdVO_4$ stoichiometric NPs. Contrary to the colorless appearance of aqueous dispersions of other neodymium-doped NPs,[14] the $NdVO_4$ colloidal dispersion presents an evident blue color. This reveals, simultaneously, a strong absorption in the visible (caused by the large Nd^{3+} content per NPs) and a negligible optical scattering (thanks to their reduced size and the absence of particle agglomeration, which is demonstrated in the DLS results shown in the Supporting Information, section S3). The superior optical absorption of $NdVO_4$ stoichiometric NPs when compared to previously used Nd^{3+}-doped PT-NPs is evidenced in **Figure 1(b)** that includes, for the sake of comparison, the absorption spectrum of an aqueous solution of Nd:LaF_3 NPs at a concentration of 10% in mass. The neodymium concentration in Nd:LaF_3 NPs was set to 5.6 at.%, being this the maximum neodymium content that could be incorporated without compromising their morphological quality or their colloidal stability (this is why 5.6 at.% doped Nd:LaF_3 NPs were considered in previous works as "heavily-doped" NPs). As can be observed, the absorption of our $NdVO_4$ NPs is markedly larger than that of the heavily-doped Nd:LaF_3 NPs that have been successfully used as photothermal agents.[16] From the absorption spectrum included in **Figure 1(c)** we have estimated a peak absorption cross section per NP mass close to 75 $cm^2 \cdot g^{-1}$ for the $NdVO_4$ stoichiometric NPs. This is, roughly, 20 times that estimated for the previously used Nd:LaF_3 PT-NPs (close to 3.8 $cm^2 \cdot g^{-1}$ for a neodymium concentration of 5.6 at.%) that cannot be solely explained by the different neodymium concentration (about 4 times higher in $NdVO_4$ stoichiometric NPs than in Nd:LaF_3 NPs). The difference in the absorption coefficients could be also attributed the different absorption cross sections of neodymium ions in both crystal matrices. Although these values are not known for either LaF_3 or $NdVO_4$ NPs, we can estimate it from previous works dealing with neodymium-doped LaF_3 and $NdVO_4$ crystals. The absorption cross section at ≈ 790 nm of neodymium ions in LaF_3 crystals has been found

to be close to $2.5 \cdot 10^{-20}$ cm^2 whereas the unpolarized absorption cross section at ≈ 808 nm of neodymium ions in (Gd,Y)VO_4 crystals is close to $20 \cdot 10^{-20}$ cm^2.[20] Thus the absorption cross section of neodymium ions in $NdVO_4$ NPs can be assumed to several times larger than in LaF_3 NPs, this difference also contributing to the much larger absorption coefficient per mass found for $NdVO_4$ NPs.

2.1.1. Spectroscopic characterization

In addition to their larger absorption, $NdVO_4$ NPs present an additional advantage with respect to their Nd:LaF_3 counterparts. The absorption peak wavelength of ultrasmall $NdVO_4$ NPs lies at 808 nm, where commercial cost effective diodes typically operate. This is at variance to the case of Nd:LaF_3 NPs for which the position of their absorption peak (789 nm) requires the use of specially pre-designed laser diodes. The comparison included in Figure 1(c) suggest that ultrasmall $NdVO_4$ NPs would require much lower 808 nm laser power densities to achieve the same heating effects than Nd:LaF_3.

The high neodymium content in $NdVO_4$ stoichiometric NPs, which results in an extremely high absorption cross section, also affects their luminescence properties. Heavily-doped NPs typically produce much lower fluorescence signals than NPs with lower contents of neodymium ions, due to the well-known emission concentration quenching. Despite their extremely high neodymium content, the $NdVO_4$ NPs still present a bright fluorescence signal, as is evidenced in the inset of **Figure 2(a)** that shows the infrared (900-1700 nm) image of a colloidal suspension of $NdVO_4$ NPs (0.6% mass concentration). The emission spectrum obtained under 808 nm optical excitation is shown in Figure 2(a), where the three emission bands characteristic of Nd^{3+} ions at around 890, 1060 and 1300 nm (corresponding to transitions $^4I_{9/2} \rightarrow {}^4F_{3/2}$, $^4I_{11/2} \rightarrow {}^4F_{3/2}$ and $^4I_{13/2} \rightarrow {}^4F_{3/2}$, respectively) can be clearly seen. As we mentioned before, all these bands lie in the biological windows, making these NPs

particularly suitable for deep-tissue fluorescence bioimaging. [10, 15c, 21] **Figure 2(b)** includes the fluorescence decay curve of the colloidal solution of $NdVO_4$ NPs as obtained under 808 nm, 10 ns optical pulsed excitation. The decay curve was found to follow a single exponential decay with a fluorescence lifetime value as low as 150 ns. Both the single exponential character and the reduced fluorescence lifetime value can be explained by taking into account different factors. First of all, the ultrasmall size of $NdVO_4$ NPs results in a very high surface to volume ratio, which means that a large (over 80%) proportion of Nd^{3+} atoms in a single $NdVO_4$ NP will be in the surface so that nonradiative interactions with the aqueous medium will dominate over radiative transitions.

In general, as has been demonstrated for other RENPs, smaller NP sizes result in lower QYs and therefore, in shorter lifetime values.[22] Moreover, the high neodymium content, which confers these NPs their photothermal properties, also contributes to a shortening of the fluorescence lifetime by promoting energy migration to surface ions as well as Nd^{3+}-Nd^{3+} cross relaxation nonradiative decay processes.[23] The contribution of such processes to the drastic reduction in the fluorescence lifetime found for our $NdVO_4$ stoichiometric NPs has been investigated by measuring the fluorescence decay curves of Nd^{3+}-doped $GdVO_4$ ultrasmall NPs with different doping levels. Results are included in Figure 2(b). A continuous decrease of the fluorescence lifetime with increasing Nd^{3+} content has been observed. Fluorescence lifetimes were found to be 500, 300 and 150 ns for Nd^{3+} molar doping levels of 6, 18 and 100%, respectively. The fluorescence lifetime previously reported for a 1 at.% Nd^{3+} (6 mol.%) doped $GdVO_4$ bulk crystal was close to 80 μs,28 i.e. close to 160 times the fluorescence lifetime obtained for $GdVO_4$ ultrasmall NPs with the same doping level. This reduction is unequivocally related to the large surface-to-volume ratio characteristic of NPs and it does not obey to Nd^{3+}-Nd^{3+} interactions that are assumed to be present in both bulk and nanosized crystals. On the other hand, increasing the Nd^{3+} doping level from 6 up to 100 mol.% causes an additional four fold reduction in the fluorescence lifetime. We can, therefore,

conclude that the main cause of the short fluorescence lifetimes found for ultrasmall $NdVO_4$ NPs is the nonradiative decay taking place at the NPs surface.[24]

In order to estimate the contribution of the nonradiative decay to the light-to-heat conversion, we calculated the photothermal conversion efficiency, η, of our NPs as is described in detail in section S2 of the Supporting Information. The photothermal conversion efficiency, defined as the fraction of the absorbed power that is transformed into heat, has been calculated by monitoring the temperature during a cycle of laser-induced heating and subsequent cooling of an aqueous dispersion of NPs using expression (1), as is described in the literature.[25]

$$\eta = \frac{hA(T_{max}-T_0)-Q_0}{I(1-10^{-DO})} \quad (1)$$

where h is the heat transfer coefficient and A, the surface area of the container where the solution is placed, while T_{max} and T_0 represent the maximum temperature reached by the dispersion containing the NPs and the temperature at the surroundings, respectively. Q_0 corresponds to the heat dissipated from the light absorbed by the solvent and container, I to the laser power and OD to the optical density of the sample. Using the procedure found in the literature and described in section S4, we found a photothermal conversion efficiency η = 72.1 % at an excitation wavelength of 808 nm. This is among the highest photothermal conversion efficiencies reported for nanosized photothermal agents, as is evidenced in Table S1 in the Supporting Information.

We also investigated the wavelength dependence of the laser-induced heating of an aqueous suspension of $NdVO_4$ NPs under optical excitation by a 780-830 nm tunable Ti:Sapphire laser. For each wavelength a thermographic image of the colloidal solution was recorded. The obtained results are summarized in **Figure 3**, where three representative thermographic images obtained upon laser excitation at 790, 808 and 820 nm, respectively, are shown (**Figure 3(a)**). **Figure 3(b)**, in which the maximum steady state temperature increment is represented as a function of the irradiation wavelength, reveals that the maximum heating occurs at 808 nm, in good accordance with the position of the absorption peak (see Figure

1(c)). Indeed, the heating spectrum included in Figure 3(b) well reproduces the spectral shape of the absorption spectrum of $NdVO_4$ NPs. This unequivocally indicates that the light-to-heat conversion efficiency of the colloidal dispersion is governed by the optical absorption of $NdVO_4$ NPs.

In order to compare the heating efficiency of our $NdVO_4$ stoichiometric NPs with their Nd:LaF_3 PT-NPs counterparts, we analyzed their heating performance in ex vivo experiments. A chicken breast tissue sample was injected at 2 mm depth with 100 µL of an aqueous dispersion of $NdVO_4$ NPs at a mass concentration of 10%. The tissue was then irradiated with different 808 nm laser intensities and thermographic images, such as the ones shown in **Figure 4(a)**, were collected in order to determine the light-induced temperature increment at the tissue surface. Results are included in **Figure 4(b)**. The tissue temperature increases linearly with the laser intensity, with a slope close to 12 $^{o}C \cdot cm^2 \cdot W^{-1}$. For the sake of comparison, the temperature vs laser power slopes obtained in the past by using heavily-doped (5.6% at.) Nd:LaF_3 NPs under similar conditions have also been schematically included in Fig. 4(b).[26] At this point it should be noted that, although the same diode laser was used in both cases, for experiments involving the Nd:LaF_3 NPs the diode wavelength was temperature tuned down to 802 nm in order to increase the optical absorption of Nd:LaF_3 NPs (whose absorption spectrum peaks at 790 nm).[27] As we mentioned before, Nd:LaF_3 NPs have been successfully used as therapeutic photothermal agents, however, their heating curve has a less pronounced slope (below 5 $^{o}C \cdot cm^2 \cdot W^{-1}$).[15a, 16] It is important to note that the heating efficiency of Nd:LaF_3 NPs would be about 80% higher if the excitation wavelength matched the absorption peak (≈ 789 nm).[16] However, even after wavelength optimization, the heating efficiency of Nd:LaF_3 would still be lower than that of $NdVO_4$ NPs. This could be explained in terms of the larger absorption cross section of the $NdVO_4$ NPs, as has been previously discussed, and also in terms of a larger the fractional thermal loading (fraction of the absorbed energy that is converted into heat) of $NdVO_4$ NPs, which is known to increase

with neodymium concentration in a nonlinear way.[16] At this point, we should note that the fact that the optimum excitation wavelength of $NdVO_4$ NPs is 808 nm instead of 790 nm is an additional advantage, as 790 nm radiation has been demonstrated to be much more harmful to cells than 808 nm radiation.[12]

The superior heating efficiency of ultrasmall $NdVO_4$ stoichiometric NPs indicates that using them as photothermal agents for tumor treatments would substantially reduce the optical excitation densities required for efficient treatment when compared to previously used neodymium-doped PT-NPs. This, in turn, would lead to a significant reduction in the magnitude and extension of the undesirable collateral damage.

The potential ability of ultrasmall $NdVO_4$ stoichiometric NPs for simultaneous laser-induced heating and imaging was finally tested in an animal model (in vivo). For that purpose, a CD1 mouse was subcutaneously injected with 100 μL of a concentrated dispersion of $NdVO_4$ NPs (10% mass concentration) in TBS (tris-buffered saline), corresponding to a total injected NP mass of 10 mg. Accurate localization of the subcutaneous injection of $NdVO_4$ NPs was achieved by measuring an infrared (> 1000 nm) fluorescence image of the mouse by using an InGaAs CCD camera. Optical excitation was performed with an 808 nm laser diode providing an excitation power density of 0.6 $W \cdot cm^{-2}$. **Figure 5(a)** shows an optical picture of the mouse in which the injection site is marked by an arrow. The infrared fluorescence image of the subcutaneously injected mouse is included in **Figure 5(b)**, from which is clear that, even at this low laser power density, the injected $NdVO_4$ NPs produce a bright fluorescence signal. The merge of both images is shown in **Figure 5(c)**, in which the spatial overlap between the fluorescence signal and subcutaneous injection is evidenced. **Figures 5(a)-(c)** reveal the potential use of $NdVO_4$ infrared fluorescence for subtissue imaging with moderate 808 nm excitation densities, achievable with an inexpensive commercial laser diode. The same laser excitation intensity was applied to the mouse for 4 minutes while continuously monitoring the skin temperature with an infrared thermographic camera. The obtained results

are summarized in **Figure 5**. The time evolution of the surface temperature during a 4-minute long irradiation is represented in **Figure 5(d)**, registering a skin temperature increment around 17 ºC. Such laser-induced heating was found to be well localized at injection site as it is evidenced in the thermographic image included as an inset in **Figure 5(d)**, which was recorded 4 minutes after starting the 808 nm laser irradiation.

It has been demonstrated that during NP-PTT treatments the skin temperature does differ from that of the exact point where the injected volume is located. In particular, it has already been demonstrated that the difference between skin and injection site temperatures could be as high as 60 %.[15a] In our particular case, this means that even at lower 808 nm laser intensities the temperature at the injection site could reach temperatures of 50 ºC and higher, as required for tumor ablation.[28] It should be noted at this point that the 808 nm power density here used (0.6 $W \cdot cm^{-2}$) is well below the power densities previously used in photothermal therapies of cancer tumors also based on neodymium-doped NPs (typically above 1 $W \cdot cm^{-2}$) where a non-negligible heating of non-targeted tissues was evidenced.[4b, 29] Indeed, such a low irradiation intensity is comparable to that previously used during the minimally invasive photothermal therapies of cancer tumors based on carbon nanostructures.[30] Consequently, ultrasmall $NdVO_4$ stoichiometric nanoparticles emerge as a strong alternative to the traditionally used photothermal agents such as carbon based nanostructures and metallic nanoparticles.

Although these results point out that $NdVO_4$ nanoparticles are good candidates for in vivo photothermal therapy, before carrying out further experiments in animal models, a thorough evaluation of their toxicity needs to be performed. While this is the case for any material intended for use in biomedicine, this is even more so the case with these NPs as $NdVO_4$ nanostructures have been reported to show photocatalytic activity, which would cause the production of free radicals upon illumination.[31] Despite this fact, the preliminary in vitro toxicity studies we have performed revealed no significant toxic effects for NP concentrations up to 500 μg/mL and incubation times as long as 6 hours, as can be seen in **Figure 6**.

However, further systematic and in depth in vitro studies need to be performed before definitely ruling out NP-associated toxicity.

3. Conclusion

In summary, we have demonstrated that the unique combination of optical properties of ultrasmall $NdVO_4$ stoichiometric nanoparticles (808 nm centered absorption band, reduced QY yield –which implies a high heating capacity-, negligible scattering cross section) make them excellent candidates to be used as multifunctional agents for in vivo photothermal cancer therapy. The results here presented prove the outstanding photothermal capabilities of the $NdVO_4$ NPs, which suggest that they could be successfully used for selective in vivo photothermal therapy using very low laser intensities, although this fact needs to be completely evaluated in real photothermal therapy in tumor-bearing mice. Moreover, the bright luminescence signal presented by these NPs in the second biological window allows for easily determining the location of the NPs through infrared fluorescence imaging and could be applied to determine the NPs location after their injection and, also, to monitor the post-treatment evolution of the tumor itself and the biodistribution and clearance of the NPs from the body.

This work introduces to the scientific community rare earth-based stoichiometric NPs as promising and unexplored photothermal agents that could be a serious alternative to the traditionally used photothermal agents such as carbon-based materials and metallic NPs with the additional advantage of their deep-tissue imaging capabilities

4. Experimental Section

Synthesis of colloidal $NdVO_4$ nanoparticles. All chemicals: neodymium (III)-nitrate hexahydrate, $Nd(NO_3)_3x6H_2O$ (99.9%, Alfa Aesar), amonium-vanadium oxide, NH_4VO_3 (min. 99.0%, Alfa Aesar), trisodium citrate (99+ %, Sigma Aldrich) and sodium-hydroxide, NaOH (min. 99%, Moss Hemos), were used without any purification. $NdVO_4$ colloidal solutions

were synthesized by the following procedure: 0.05 M solution of trisodium citrate (15 mL) is added drop by drop to the 0.05M solution of $Nd(NO_3)_3$ (20 mL) at room temperature, and white precipitate from Nd^{3+}- Cit^{3-} complex was formed. After vigorous stirring for 30 min, white precipitate is completely dissolved by the addition, drop by drop, of 0.05 M NH_4VO_3 (15 mL, dissolved in 0.15 M NaOH). The transparent and bluish solution, with pH of about 8, is subsequently heated and stirred at 60 °C for 60 min. Finally, the colloidal solution is cooled down to the room temperature. Slow growth of particles was achieved by dialysis against the water until pH = 7 of solution was reached.

Electron microscopy characterization. The size of nanoparticles were studied by high-resolution transmission electron microscopy with a Jeol ARM 200 CF, a probe Cs-corrected scanning transmission electron microscope, equipped with cold FEG electron source, operated at 200 kV. HAADF (High-angle annular dark-field) STEM (scanning transmission electron microscope) technique was used for sample imaging.

*Spectroscopic characterization***.** The absorption spectrum was measured using an UV/VIS/NIR spectrophotometer (Perkin Elmer Lambda1050). The emission spectrum was obtained under excitation with a tunable Ti:Sapphire (Spectra Physics 3900) laser working at 808 nm. The luminescence signal was collected, after passing through appropriate filters, and spectrally analyzed by an infrared Germanium detector coupled to a SPEX 500M high-resolution spectrometer. For the fluorescence lifetime measurements, a tunable pulsed optical parametric oscillator (Spectra Physics Quanta-Ray 730 MOPO) working at 808 nm was used as excitation source. The emission signal in that case was collected by a photomultiplier tube and recorded with a LeCroy digital oscilloscope.

Fluorescence imaging. Fluorescence images were collected using an InGaAs CCD camera with enhanced sensitivity in the 1000-1700 nm spectral range (XEva1.7-320). Optical excitation was achieved using a fiber-coupled 808 nm laser diode (LIMO). A long pass filter

with cut-off wavelength at 850 nm was used to remove the 808 nm pump background. Thermal images were recorded using a thermographic camera (FLIR E40bx).

Animal experiments. A 6-week-aged female CD1 mouse was subcutaneously injected with 100 μL of a 10% in mass dispersion of the nanoparticles in PBS and subjected to irradiation with an 808 nm laser diode at 0.8 $W \cdot cm^{-2}$ for three minutes so as to perform an in vivo test of the photothermal properties of the $NdVO_4$ NPs. All the experimental procedures with animals were carried out in compliance with the 2013/63/UE European guidelines and were approved by the Ethics Committee from Universidad Autónoma de Madrid (CEIT) in the frame of the project FIS- MAT2013-47395-C4-1-R supported by the Spanish Ministerio de Economía y Competitividad.

In vitro cytotoxicity studies.The MTT (3-(4,5-dimethylthiazol-2-yl)-2,5-diphenyltetrazolium bromide) assay is a simple non-radioactive colorimetric assay to measure cell cytotoxicity, proliferation or viability. MTT is a yellow, watersoluble, tetrazolium salt. Metabolically active cells are able to convert this dye into a waterinsoluble dark blue formazan by reductive cleavage of the tetrazolium ring. Formazan crystals, then, can be dissolved in an organic solvent such as dimethylsulphoxide (DMSO) and quantifed by measuring the absorbance of the solution at 540 nm, and the resultant value is related to the number of living cells. To determine cell cytotoxicity/viability, the cells were plated in a 24 well plate at 37 °C in 5% CO_2 atmosphere.

After 48 h of culture, the medium in the well was replaced with the fresh medium containing different concentrations of $NdVO_4$ NPs (100, 200, 300, 400 and 500 μg/mL) and cells were incubated for 6 hours. After incubation, the medium was removed and added completed medium without nanoparticles. After 24 h, 0.5 mL of MTT dye solution (0.05 mg/mL of MTT, Sigma) was added to each well. After 2–3 h of incubation at 37 °C and 5% CO_2, the medium was removed and formazan crystals were solubilized in 0.5 mL of DMSO (Merck) and the solution was vigorously mixed to dissolve the reacted dye. The absorbance at

540 nm was read using a microplate reader (Espectra Fluor 4, Tecan). The% of viability of cells incubated with NPs as compared to control cells (i.e., without incubation with nanoparticles) was calculated as $[A]_{test}/[A]_{control} \times 100$, where $[A]_{test}$ is the absorbance of the tested sample and $[A]_{control}$ is the absorbance of the control sample.

Supporting Information
Supporting Information is available from the Wiley Online Library or from the author.

Acknowledgements
This project has been supported by the Spanish Ministerio de Economía y Competitividad under project and MAT2013-47395-C4-1-R. B. del Rosal thanks Universidad Autónoma de Madrid for an FPI grant. Dragana Jovanović and Miroslav Dramićanin acknowledge financial support of the Ministry of Education, Science and Technological development of the Republic of Serbia (grant number 45020). Goran Dražić acknowledges the financial support of the Slovenian Research Agency (ARRS) through program no. P2-0148 and project J2-6754. Authors thanks COST action CM1403.

Received: ((will be filled in by the editorial staff))
Revised: ((will be filled in by the editorial staff))
Published online: ((will be filled in by the editorial staff))

[1] P. Wust, B. Hildebrandt, G. Sreenivasa, B. Rau, J. Gellermann, H. Riess, R. Felix, P. Schlag, *The Lancet Oncology* **2002**, *3*, 487.
[2] R. W. Habash, R. Bansal, D. Krewski, H. T. Alhafid, *Critical Reviews™ in Biomedical Engineering* **2006**, *34*.
[3] D. Jaque, L. Martinez Maestro, B. del Rosal, P. Haro-Gonzalez, A. Benayas, J. L. Plaza, E. Martin Rodriguez, J. Garcia Sole, *Nanoscale* **2014**, *6*, 9494.
[4] a) E. B. Dickerson, E. C. Dreaden, X. H. Huang, I. H. El-Sayed, H. H. Chu, S. Pushpanketh, J. F. McDonald, M. A. El-Sayed, *Cancer Letters* **2008**, *269*, 57; b) J. Robinson, K. Welsher, S. Tabakman, S. Sherlock, H. Wang, R. Luong, H. Dai, *Nano Res.* **2010**, *3*, 779; c) K. Yang, S. Zhang, G. Zhang, X. Sun, S. T. Lee, Z. Liu, *Nano Lett.* **2010**, *10*, 3318; d) K. Yang, H. Xu, L. Cheng, C. Sun, J. Wang, Z. Liu, *Adv. Mater.* **2012**, *24*, 5586.
[5] R. Weissleder, *Nat. Biotechnol.* **2001**, *19*, 316.
[6] A. M. Smith, M. C. Mancini, S. Nie, *Nat. Nanotechnol.* **2009**, *4*, 710.
[7] a) G. Hong, J. T. Robinson, Y. Zhang, S. Diao, A. L. Antaris, Q. Wang, H. Dai, *Angew. Chem., Int. Ed.* **2012**, *51*, 9818; b) T. Zako, M. Yoshimoto, H. Hyodo, H. Kishimoto, M. Ito, K. Kaneko, K. Soga, M. Maeda, *Biomaterials Science* **2015**, *3*, 59.
[8] a) F. Wang, D. Banerjee, Y. Liu, X. Chen, X. Liu, *Analyst* **2010**, *135*, 1839; b) M. Pedroni, F. Piccinelli, T. Passuello, M. Giarola, G. Mariotto, S. Polizzi, M. Bettinelli, A. Speghini, *Nanoscale* **2011**, *3*, 1456; c) F. Vetrone, R. Naccache, V. Mahalingam, C. G. Morgan, J. A. Capobianco, *Adv. Funct. Mater.* **2009**, *19*, 2924; d) T. Maldiney, G. Sraiki, B. Viana, D. Gourier, C. Richard, D. Scherman, M. Bessodes, K. Van den Eeckhout, D. Poelman, P. Smet, *Optical Materials Express* **2012**, *2*, 261.

[9] a) A. Bednarkiewicz, D. Wawrzynczyk, M. Nyk, W. Strek, *Applied physics. B, Lasers and optics* **2011**, *103*, 847; b) V. K. Tikhomirov, K. Driesen, V. D. Rodriguez, P. Gredin, M. Mortier, *Optics Express* **2009**, *17*, 11794.
[10] G. Chen, T. Y. Ohulchanskyy, S. Liu, W.-C. Law, F. Wu, M. T. Swihart, H. Ågren, P. N. Prasad, *ACS Nano* **2012**, *6*, 2969.
[11] D. Naczynski, M. Tan, M. Zevon, B. Wall, J. Kohl, A. Kulesa, S. Chen, C. Roth, R. Riman, P. Moghe, *Nat. Commun.* **2013**, *4*.
[12] K. König, H. Liang, M. W. Berns, B. J. Tromberg, *Opt. Lett.* **1996**, *21*, 1090.
[13] G. H. Dieke, H. M. Crosswhite, H. Crosswhite, *Spectra and energy levels of rare earth ions in crystals*, Interscience Publishers New York, 1968.
[14] U. Rocha, C. Jacinto da Silva, W. Ferreira Silva, I. Guedes, A. Benayas, L. Martínez Maestro, M. Acosta Elias, E. Bovero, F. C. J. M. van Veggel, J. A. García Solé, D. Jaque, *ACS Nano* **2013**, *7*, 1188.
[15] a) U. Rocha, K. Upendra Kumar, C. Jacinto, J. Ramiro, A. J. Caamaño, J. García Solé, D. Jaque, *Appl. Phys. Lett.* **2014**, *104*; b) I. Villa, A. Vedda, I. X. Cantarelli, M. Pedroni, F. Piccinelli, M. Bettinelli, A. Speghini, M. Quintanilla, F. Vetrone, U. Rocha, *Nano Res.* **2014**, 1; c) U. Rocha, K. U. Kumar, C. Jacinto, I. Villa, F. Sanz-Rodríguez, M. del Carmen Iglesias de la Cruz, A. Juarranz, E. Carrasco, F. C. J. M. van Veggel, E. Bovero, J. G. Solé, D. Jaque, *Small* **2014**, *10*, 1141.
[16] E. Carrasco, B. del Rosal, F. Sanz-Rodríguez, Á. J. de la Fuente, P. H. Gonzalez, U. Rocha, K. U. Kumar, C. Jacinto, J. G. Solé, D. Jaque, *Adv. Funct. Mater.* **2015**, *25*, 615.
[17] Y. Sato, T. Taira, *Selected Topics in Quantum Electronics, IEEE Journal of* **2005**, *11*, 613.
[18] a) Z. Xu, C. Li, Z. Hou, C. Peng, J. Lin, *CrystEngComm* **2011**, *13*, 474; b) H. Deng, S. Yang, S. Xiao, H.-M. Gong, Q.-Q. Wang, *J. Am. Chem. Soc.* **2008**, *130*, 2032; c) S. Yuvaraj, R. Kalai Selvan, V. Bhooshan Kumar, I. Perelshtein, A. Gedanken, S. Isakkimuthu, S. Arumugam, *Ultrason. Sonochem.* **2014**, *21*, 599; d) J. Liu, Y. Li, *J. Mater. Chem.* **2007**, *17*, 1797.
[19] K. Huang, H. Ma, J. Liu, S. Huo, A. Kumar, T. Wei, X. Zhang, S. Jin, Y. Gan, P. C. Wang, *ACS Nano* **2012**, *6*, 4483.
[20] a) T. Bhutta, A. Chardon, D. Shepherd, E. Daran, C. Serrano, *Quantum Electronics, IEEE Journal of* **2001**, *37*, 1469; b) T. Jensen, V. Ostroumov, J.-P. Meyn, G. Huber, A. Zagumennyi, I. Shcherbakov, *Applied Physics B* **1994**, *58*, 373.
[21] I. Villa, A. Vedda, I. Cantarelli, M. Pedroni, F. Piccinelli, M. Bettinelli, A. Speghini, M. Quintanilla, F. Vetrone, U. Rocha, C. Jacinto, E. Carrasco, F. Rodríguez, Á. Juarranz, B. del Rosal, D. Ortgies, P. Gonzalez, J. Solé, D. García, *Nano Res.* **2015**, *8*, 649.
[22] J.-C. Boyer, F. C. Van Veggel, *Nanoscale* **2010**, *2*, 1417.
[23] F. Träger, *Springer handbook of lasers and optics*, Springer Science & Business Media, 2007.
[24] G. A. Kumar, C. W. Chen, J. Ballato, R. E. Riman, *Chem. Mater.* **2007**, *19*, 1523.
[25] a) Q. Tian, F. Jiang, R. Zou, Q. Liu, Z. Chen, M. Zhu, S. Yang, J. Wang, J. Wang, J. Hu, *ACS Nano* **2011**, *5*, 9761; b) V. P. Pattani, J. W. Tunnell, *Lasers in Surgery and Medicine* **2012**, *44*, 675.
[26] U. Rocha, K. Upendra Kumar, C. Jacinto, J. Ramiro, A. J. Caamaño, J. García Solé, D. Jaque, *Appl. Phys. Lett.* **2014**, *104*, 053703.
[27] B. del Rosal, A. Pérez-Delgado, M. Misiak, A. Bednarkiewicz, A. S. Vanetsev, Y. Orlovskii, D. J. Jovanović, M. D. Dramićanin, U. Rocha, K. U. Kumar, *J. Appl. Phys.* **2015**, *118*, 143104.
[28] R. W. Habash, R. Bansal, D. Krewski, H. T. Alhafid, *Critical Reviews™ in Biomedical Engineering* **2006**, *34*.

[29] L. M. Maestro, P. Haro, B. del Rosal, J. Ramiro, A. J. Caamaño, F. Sanz-Rodríguez, A. Juarranz, E. Carrasco, J. G. Solé, D. Jaque, *Nanoscale* **2013**.
[30] a) K. Yang, J. Wan, S. Zhang, B. Tian, Y. Zhang, Z. Liu, *Biomaterials* **2012**, *33*, 2206; b) N. N. Huang, H. Q. Wang, J. H. Zhao, H. Lui, M. Korbelik, H. S. Zeng, *Lasers in Surgery and Medicine* **2010**, *42*, 638.
[31] J. Xu, C. Hu, G. Liu, H. Liu, G. Du, Y. Zhang, *J. Alloys Compd.* **2011**, *509*, 7968.

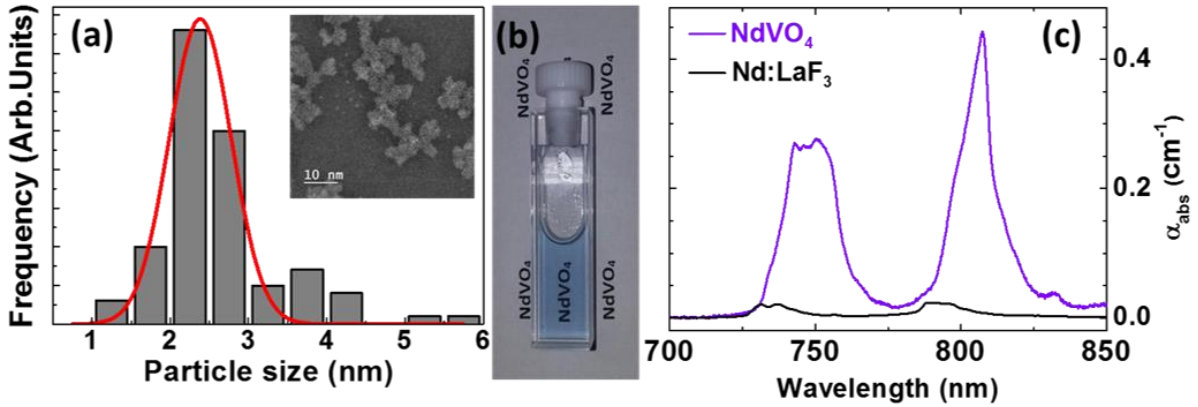

Figure 1. (a) Size histogram of the $NdVO_4$ stoichiometric nanoparticles as obtained from the high resolution TEM included as an inset. **(b)** Optical picture of an aqueous dispersion of $NdVO_4$ stoichiometric nanoparticles at a mass concentration of 0.6%. The blue color reveals a strong optical absorption in the visible due to Nd^{3+} ions. **(c)** Absorption spectrum of the colloidal dispersion shown in (b). The absorption spectrum of an aqueous dispersion of heavily-doped (5.6 at.%) Nd:LaF_3 at the same concentration is included for comparison.

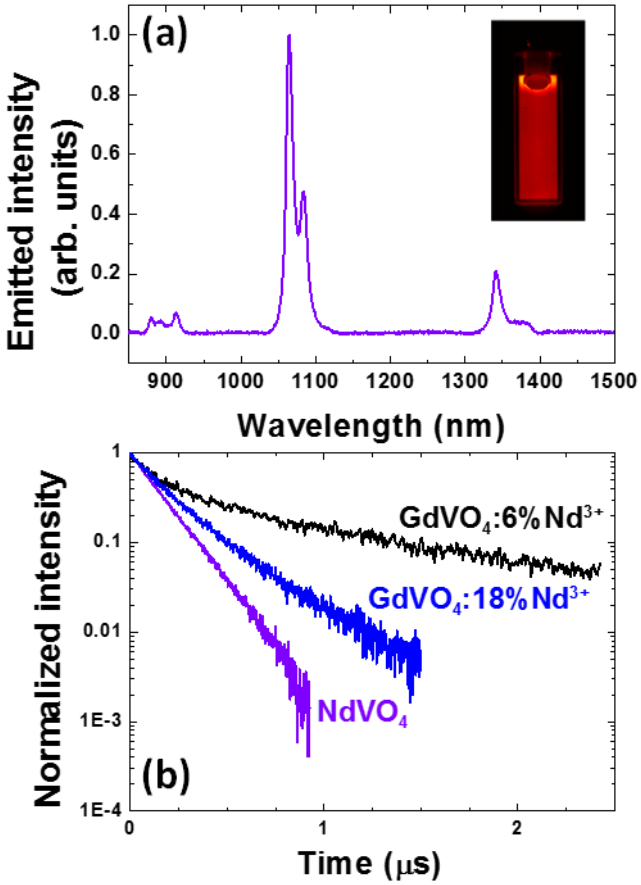

Figure 2. (a) Emission spectrum of a colloidal dispersion of $NdVO_4$ (0.6 % mass concentration) obtained under optical excitation at 808 nm. The inset shows the infrared (900-1700 nm) fluorescence image of the colloidal solution under 808 nm optical excitation as obtained with an InGaAs camera. **(b)** Fluorescence decay curve as obtained from a colloidal solution of $NdVO_4$ nanoparticles. The decay curves obtained for 6 mol.% and 18 mol.% Nd^{3+}-doped $GdVO_4$ ultrasmall NPs have been included for comparison.

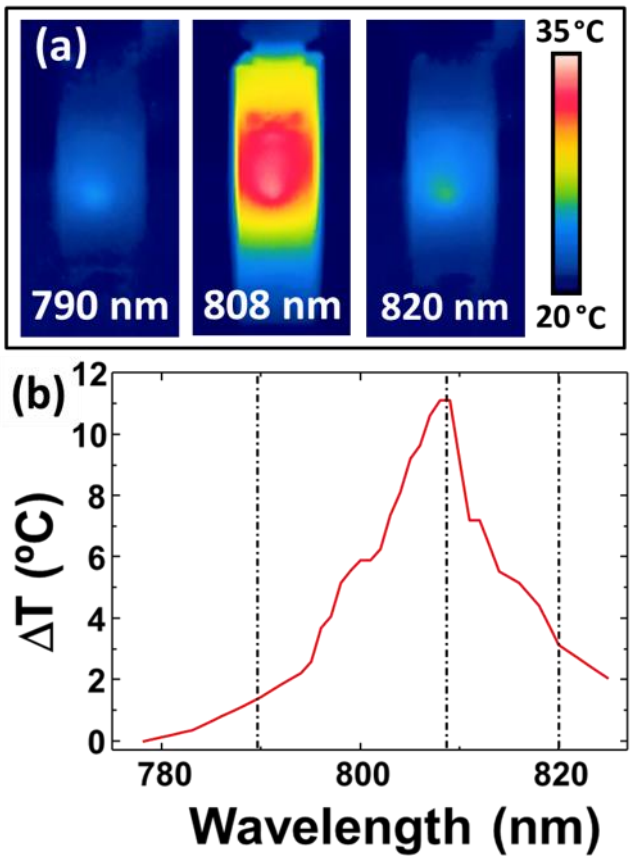

Figure 3. (a) Thermal images of a quartz cuvette containing a colloidal solution of $NdVO_4$ at a 0.6 % mass concentration under optical excitation at three different wavelengths. **(b)** Maximum temperature increment produced in the colloidal solution as a function of the laser wavelength. A clear maximum is observed at 808 nm, in agreement with the peak position in the absorption spectrum.

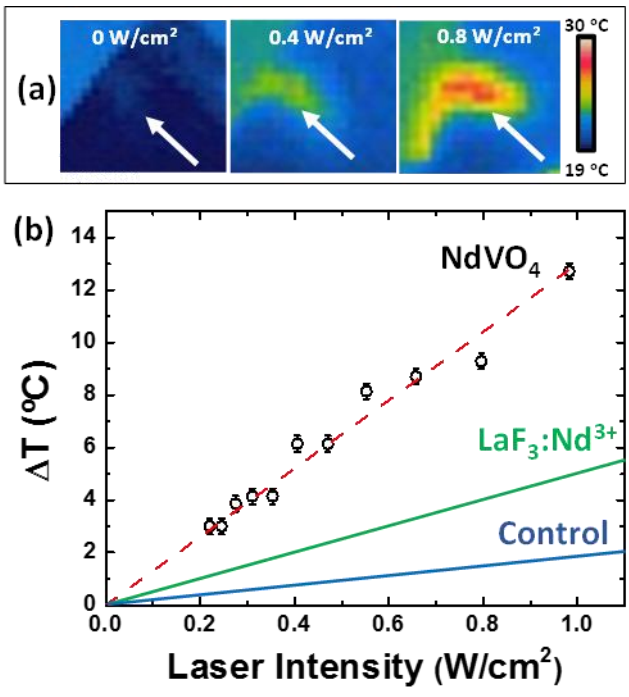

Figure 4. (a) Thermal images of a subcutaneous injection (~2 mm depth) of $NdVO_4$ nanoparticles in chicken tissue as obtained for different 808 nm laser excitation intensities. Arrows indicate the location of the $NdVO_4$ injection. **(b)** Maximum tissue surface temperature as a function of the 808 nm laser intensity. Dots are experimental data and dashed line is the best linear fit. The maximum tissue surface temperature obtained under the same experimental conditions with an injection of heavily-doped Nd:LaF_3 (green line) and in the control case (blue line) are included for the sake of comparison.

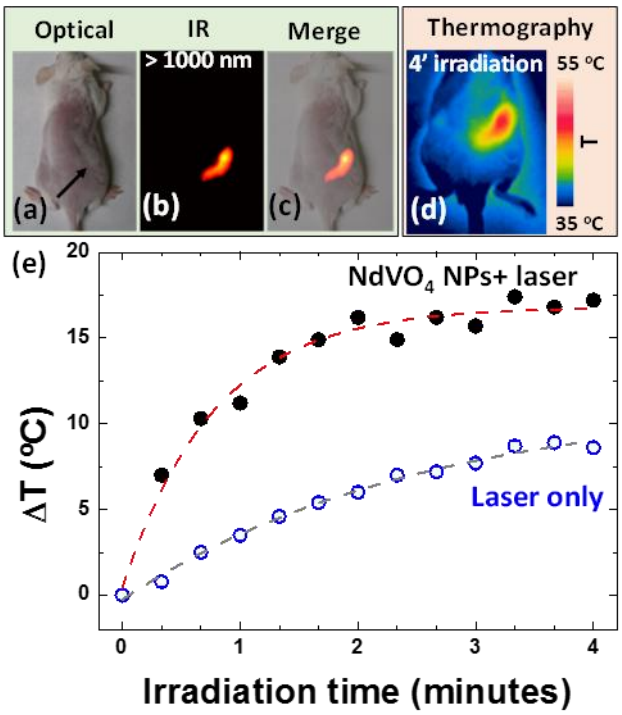

Figure 5. (a) Optical image of a CD1 mouse subcutaneously injected with 100 µL of an aqueous dispersion of $NdVO_4$ stoichiometric NPs at (10% mass concentration). The arrow indicates the location of the injection. **(b)** Infrared fluorescence image of the same mouse as in (a) as obtained under 808 nm, 0.2 $W \cdot cm^{-2}$ excitation with an AsGaIn camera before which a 1000 nm longpass filter was placed. **(c)** Merge of (a) and (b) revealing fluorescence contrast only at the injection site. **(d)** Thermographic image of the mouse after 4 minutes under irradiation at 808 nm (0.6 $W \cdot cm^{-2}$). Note that the maximum heating corresponds to the injection site **(e)** Time evolution of the surface (skin) temperature at the injection site (black dots) and in a control mouse (blue dots) after switching on the 808 nm laser (0.6 $W \cdot cm^{-2}$). Dashed lines are guides for the eyes.

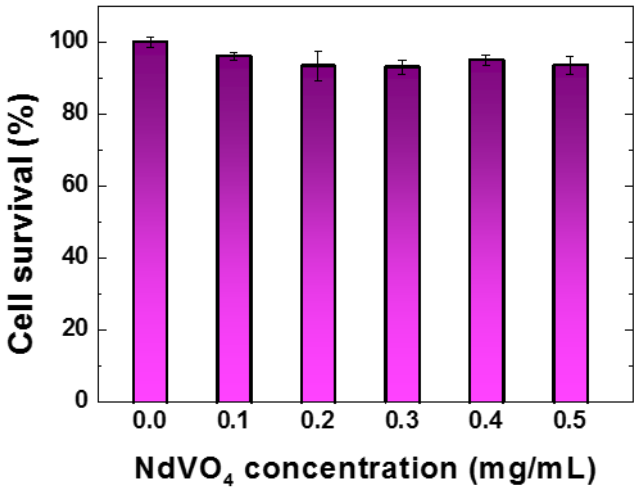

Figure 6. Fraction of surviving HeLa cells (%) after incubation for 6 hours with different concentrations of $NdVO_4$ nanoparticles. Error bars correspond to the standard deviation.

IR-emitting $NdVO_4$ ultrasmall NPs show a remarkable photothermal conversion efficiency (72.1%) under 808 nm irradiation, which makes them particularly interesting for combined photothermal therapy and bioimaging. Their outsanding light-to-heat conversion capability, studied ex vivo and in vivo, would allow for photothermal treatments at laser intensities much lower than the ones used up to this moment with fluorescent rare earth-based nanomaterials.

B. del Rosal, A. Pérez-Delgado, E. Carrasco, D. Jovanović, M. D. Dramićanin, G. Dražić, A. Juarranz de la Fuente, F. Sanz-Rodríguez, and D. Jaque*

Neodymium-based stoichiometric ultrasmall nanoparticles for multifunctional deep-tissue photothermal therapy

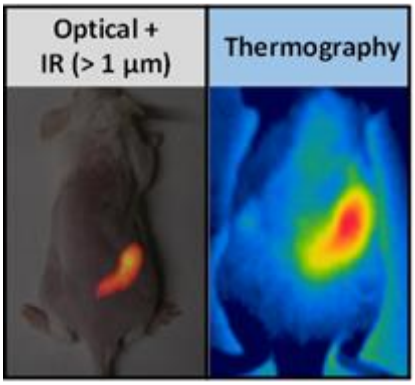

ToC figure ((Please choose one size: 55 mm broad × 50 mm high **or** 110 mm broad × 20 mm high. Please do not use any other dimensions))